

Hanbury Brown-Twiss Interferometry for Fractional and Integer Mott Phases

Ana Maria Rey¹, Indubala I. Satija^{2,3} and Charles W. Clark²

¹ *Institute for Theoretical Atomic, Molecular and Optical Physics, Cambridge, MA, 02138, USA*

² *National Institute of Standards and Technology, Gaithersburg MD, 20899, USA and*

³ *Dept. of Phys., George Mason U., Fairfax, VA, 22030, USA*

(Dated: May 3, 2018)

Hanbury-Brown-Twiss interferometry (HBTI) is used to study integer and fractionally filled Mott Insulator (MI) phases in period-2 optical superlattices. In contrast to the quasimomentum distribution, this second order interferometry pattern exhibits high contrast fringes in the *insulating phases*. Our detailed study of HBTI suggests that this interference pattern signals the various superfluid-insulator transitions and therefore can be used as a practical method to determine the phase diagram of the system. We find that in the presence of a confining potential the insulating phases become robust as they exist for a finite range of atom numbers. Furthermore, we show that in the trapped case the HBTI interferogram signals the formation of the MI domains and probes the shell structure of the system.

PACS numbers: 71.30.+h, 03.75.Lm, 42.50.Lc

I. INTRODUCTION

Cold atoms in optical lattices are becoming ideal many-body systems to attain laboratory demonstrations of model quantum Hamiltonians due in part to the dynamical experimental control of the various parameters at a level unavailable in more traditional condensed matter systems. Recent experiments with bosonic atoms have been able to simulate effective one dimensional systems [1, 2, 3, 4, 5], to enter the strongly correlated Tonks Girardeau (TG) regime [2, 3] predicted many years ago [6] and to realize the superfluid to Mott insulator (MI) [7] transition by tuning the lattice parameters [8]. In fact, one of the most active frontier in cold atom systems is to explore the possibility of creating new quantum phases [9]. The capability to physically create them demands sophisticated diagnostic tools for their characterization and actual observation in the laboratory. In this paper, we use second order interference techniques, namely the Hanbury Brown and Twiss interferometry [10] to describe the rich phase diagram of interacting bosonic atoms in the presence of two competing lattices.

Multiple well super-lattices have been experimentally realized by superimposing two independent optical lattices with different periodicities [11, 12]. Recent theoretical studies of the many-body Bose-Hubbard (BH) Hamiltonian in the presence of an additional superlattice [13, 14, 15, 16, 17, 18] have centered mostly on the detailed phase diagrams of the system. The focus of this paper is to characterize the different phases of the system by analyzing the four and two point correlations that can be extracted from the time of flight images. Our study is confined to period-2 superlattices, the simplest example of a system exhibiting almost all the key aspects of a more general period- m lattices.

The HBTI technique measures second order correlations from the shot-noise density fluctuations in the absorption images of expanding atomic gas clouds. This technique has been shown [19, 20, 21] to be particularly suited for probing many-body states of cold atomic systems, as it provides complementary information to the first-order correlations inferred from the average density distribution in the absorption images. For

example, cold bosonic atoms in the MI regime do not exhibit first order interference pattern but they do have sharp second-order Bragg peaks which reflect the spatial periodicity of the lattice. The interference peaks are the manifestation of the enhanced probability for simultaneous detection of two bosons (bunching) due to the Bose-Einstein statistics.

The phase diagram of interacting bosons in the presence of 1D superlattices is landscaped by various quantum phases. Transitions to the different phases can be driven either by changing the ratio between the three sets of energy scales in the system: the interaction energy U , the tunneling rate J and the lattice modulation λ or by varying the filling factor ν . The lattice modulation induces additional fractional MI phases that occur at filling factors commensurate with the periodicity of the combined superlattice. These phases can be understood in the hard core boson (HCB) limit where the strongly interacting bosons can be mapped to noninteracting fermions. The superlattice fragments the single particle spectrum, inducing band gaps. The filling of a sub-band at a critical filling factor in the fermionic system results in a band insulator state that corresponds to a fractionally filled MI state of the bosonic atoms. The fractional MI phases survive in the soft core boson limit beyond a critical value of the interaction energy U .

Besides the fractional Mott phases, the interplay between the interaction energy and the superlattice potential can also lead to a new type of integer-filled Mott phases which cannot be understood in any special limit such as the HCB limit or the pure periodic case as they appear at finite U values and for finite strengths of the superlattice potential. These insulating phases are characterized by a modulated density profile and hence will be referred as *staggered Mott* phases.

Here we demonstrate that HBTI provides definite means to monitor the various superfluid to MI transitions and we use it as a method to obtain the phase diagram. Firstly, for a fixed U , J and λ we vary ν , and find that the onset to the transition is accompanied by a change in the sign of the superlattice induced Bragg peaks as the filling factor is increased beyond the critical ones. Secondly, for a fixed filling factor ν and fixed λ/J , we change the ratio U/J across the transitions and show

that they are signaled by a sharp maximum in the intensities of the Bragg interference peaks. We show that the phase diagram obtained from HBTI is in qualitative agreement with the recently reported phase diagram calculated from Monte-Carlo simulations [14, 15, 16, 17, 18] and with a mean field phase diagram that we derive analytically.

Another important aspect of our study is to investigate the effects of a harmonic trap on the various phases. In contrast to the translationally invariant system where the transition to insulating phases occurs only at critical filling factors, the parabolic confinement allows for the formation of fractional and integer filled MI domains in a finite window of fillings. We show that harmonically confined superlattices in the HCB limit develop a shell structure [22] analogous to the one observed in the absence of any lattice modulation at moderate values of the interaction. The HBTI interferogram provides clear signature of the formation of the different Mott domains.

The paper is organized as follows. In Sec. II we define noise correlations and the model Hamiltonian used in our study. In Sec. III, we calculate two and four-point correlations in the HCB case. In Sec. IV, we consider the BH system for finite values of interaction. We first analytically calculate the phase diagram by using mean field theory (whose details are described in Appendix A) and compare it with the phase diagram obtained from noise correlations. These higher order correlations are calculated by numerical diagonalization of the BH Hamiltonian. In Sec. V, we discuss the effects of the harmonic trap in the HCB limit. In Sec. VI we state our conclusions.

II. NOISE CORRELATIONS

In a typical experiment, atoms are released by turning off the external potentials. The atomic cloud expands, and is photographed after it enters the ballistic regime. Assuming that the atoms are noninteracting from the time of release, properties of the initial state can be inferred from the spatial images [13, 19, 23]: the column density distribution image reflects the initial quasimomentum distribution, $n(Q)$, and the density fluctuations, namely the *noise correlations*, reflect the quasimomentum fluctuations, $\Delta(Q, Q')$,

$$\hat{n}(Q) = \frac{1}{L} \sum_{j,k} e^{iQa(j-k)} \hat{a}_j^\dagger \hat{a}_k, \quad (1)$$

$$\Delta(Q, Q') \equiv \langle \hat{n}(Q) \hat{n}(Q') \rangle - \langle \hat{n}(Q) \rangle \langle \hat{n}(Q') \rangle. \quad (2)$$

In Eq. (2) we have assumed that both Q, Q' lie inside the first Brillouin zone. Here L is the number of lattice sites and a the lattice constant. In this paper, for simplicity, we focus on the quantity $\Delta(Q, 0) \equiv \Delta(Q)$. In our discussion below, N denotes the number of particles in the system and $\nu = N/L$ is the filling factor. In this paper, we will confine ourselves to the case with $\nu \leq 1$.

The BH Hamiltonian describes bosons in optical lattices when the lattice is loaded in such a way that only the lowest vibrational level of each lattice site is occupied and tunneling occurs only between nearest-neighbor sites [22]. The 1D BH

Hamiltonian in the presence of a period 2-superlattice is given by

$$\hat{H} = -J \sum_{\langle i,j \rangle} \hat{a}_i^\dagger \hat{a}_j + \frac{U}{2} \sum_j \hat{n}_j (\hat{n}_j - 1) + \sum_j 2\lambda \cos(\pi j) \hat{n}_j + \sum_j \Omega j^2 \hat{n}_j. \quad (3)$$

Here \hat{a}_j is the bosonic annihilation operator of a particle at site j , $\hat{n}_j = \hat{a}_j^\dagger \hat{a}_j$, and the sum $\langle i, j \rangle$ is over nearest neighbors. The hopping parameter J , and the on-site interaction energy U are functions of the lattice depth. The cosine term describes the onsite potential generated by the additional lattice with twice the periodicity of the main lattice. Here the main lattice creates the tight-binding system and the second lattice is assumed to be a weak perturbation. In this case atoms in the super-lattice have a hopping parameter which is independent of the lattice position. The parameter λ is almost proportional to the depth (in recoil units of the main lattice) of the additional lattice (see Ref. [11] for details). The last term takes into account the parabolic potential with Ω proportional to the parabolic trapping frequency.

III. HARD CORE LIMIT

In the strongly correlated regime, when $U \rightarrow \infty$, the BH Hamiltonian can be replaced by the HCB Hamiltonian [25],

$$\hat{H}^{(HCB)} = -J \sum_j (\hat{b}_j^\dagger \hat{b}_{j+1} + \hat{b}_{j+1}^\dagger \hat{b}_j) + \sum_j 2\lambda \cos(\pi j) \hat{n}_j + \sum_j \Omega j^2 \hat{n}_j. \quad (4)$$

Here \hat{b}_j is the annihilation operator at the lattice site j which satisfies $[\hat{b}_i, \hat{b}_j^\dagger] = \delta_{ij}$, and the on-site conditions $\hat{b}_j^2 = \hat{b}_j^{\dagger 2} = 0$, which suppress multiple occupancy of lattice sites.

HCB operators can be linked to spin-1/2 operators by means of the Holstein-Primakoff transformation [24], which maps bosonic operators into spin operators. The Holstein-Primakoff transformation maps the HCB Hamiltonian into the XY spin-1/2 Hamiltonian. The latter can in turn be mapped onto a spinless fermion Hamiltonian by means of the Jordan-Wigner transformation [25, 26].

The Bose-Fermi correspondence can be used to calculate various many-body observables of the strongly interacting bosonic system in terms of the ideal fermionic two-point functions which can be written as $g_{lm} = \sum_{k=0}^{N-1} \psi_l^{*(k)} \psi_m^{(k)}$. Here $\psi_j^{(k)}$ are the amplitudes of the single atom eigenfunctions at site j and $E_{(k)}$ are the single atom eigenenergies:

$$-J(\psi_{j+1}^{(k)} + \psi_{j-1}^{(k)}) + 2\lambda \cos(\pi j) \psi_j^{(k)} + \Omega j^2 \psi_j^{(k)} = E_{(k)} \psi_j^{(k)}. \quad (5)$$

The single-particle spectrum of period-2 superlattice can be obtained by decimating every other site of the tight binding

Eq. (5). The renormalized system at even or odd sites is described by

$$J^2(\psi_{j+2}^{(k)} + \psi_{j-2}^{(k)}) + (2J^2 + 4\lambda^2)\psi_j^{(k)} = E_{(k)}^2 \psi_j^{(k)}. \quad (6)$$

Assuming periodic boundary conditions, the eigenenergies are then given by

$$E_{(k)} = \pm 2\sqrt{J^2 \cos\left(\frac{4\pi k}{L}\right) + \lambda^2}, \quad (7)$$

where $k = 0, 1, \dots, L/2$. The effect of the additional lattice potential is to split the band into two different sub-bands, each with band-width $2\sqrt{J^2 + \lambda^2} - 2\lambda$, separated by an energy gap of 4λ .

Local observables such as the density distribution and energies are identical for the HCB and non-interacting fermionic systems. For example, the HCB ground state energy corresponds to the sum of the first N single-particle eigenstates. On the other hand, fermions and HCBs possess different non-local correlation functions. A general formulation to calculate HCB two-point correlations has been developed by Lieb and Mattis [26]. In our earlier studies [23], we have generalized Lieb and Mattis formalism and have obtained explicit formulas, involving multiple Töplitz-like determinants, to compute the four-point correlation functions required to calculate noise correlations in HCBs. The evaluation of these determinants, whose order scales with the size of the system, is in general complicated and therefore an analytical treatment is difficult. Below we will describe the results obtained by numerical computation of the explicit formulas discussed in our earlier study. For information about the exact formulas and various other relevant details we refer the readers to our earlier paper [23].

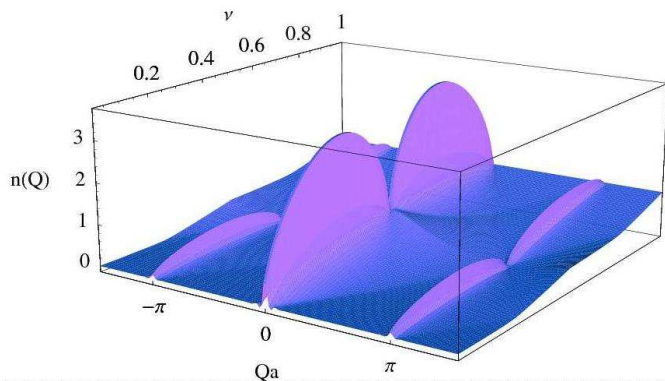


FIG. 1: Quasimomentum distribution as a function of the filling factor. The calculations were done for a system with $\lambda/J = 1$, $L = 80$ and boxed-like boundary conditions

Figs. 1 and 2 show the quasimomentum distribution and the noise correlations for all filling factors, $0 \leq \nu \leq 1$. The quasimomentum distribution exhibits interference peaks at the reciprocal lattice vectors of the combined superlattice: a large peak at $Q = 0$ and somewhat weaker peaks at $Qa = \pm\pi$, induced by the period two modulation. The peaks are a manifestation of the quasi-long-range coherence of the system. At

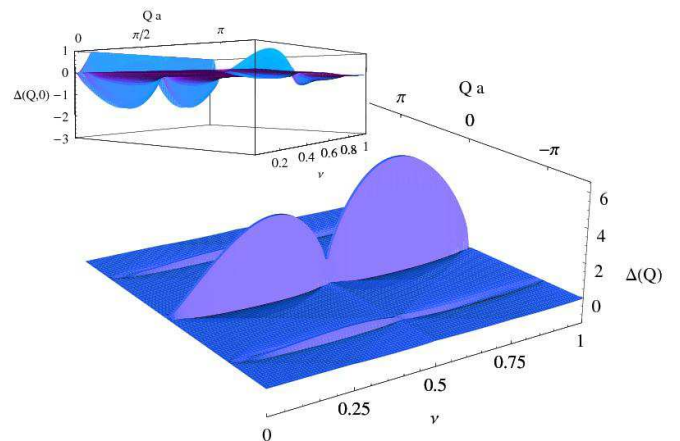


FIG. 2: Noise interference pattern as a function of the filling factor for a system with $\lambda/J = 1$, $L = 80$ and boxed-like boundary conditions. In the inset we truncated the central peak to make the negative background and the peak to dip transition more visible

$\nu = 1/2$ and 1 the first order interference pattern flattens out, signaling the insulating character of the system at these critical fillings.

The peaks at $Qa = 0$ and $\pm\pi$ also exist in the noise interference pattern (Fig.2), where they are narrower and are accompanied by adjacent satellite dips, immersed in a negative background. These satellite dips are the signatures of the long range coherence in the second order pattern as they disappear in the insulating phases (see detailed discussion in Ref.[23]). The satellite dips are clearly seen in the inset. In contrast to the quasimomentum distribution, the peaks at reciprocal lattice vectors continue to exist at the critical filling factors in the HBTI pattern. However, their intensity is strongly reduced compared to the intensity at other filling factors.

To highlight the signatures of the insulating phases in the noise correlations, we plot in Fig. 3 the visibility of the central and superlattice induced peaks. We define the visibility as the intensity of the second order Bragg fringes (noise-correlations) normalized with respect to the quasimomentum distribution:

$$\mathcal{V}(Q) \equiv \frac{\Delta(Q, 0)}{n(Q)n(0)} \quad (8)$$

The visibility $\mathcal{V}(Q)$ is a relevant experimental quantity as the normalization procedure filters some of the technical noise introduced during the measurements.

In the visibility figure one observes the development of very sharp peaks at the critical fillings. In addition, an interesting definitive signal of the fractional insulating phase is a change in the sign of the intensity of the superlattice induced peaks: as the filling factor is increased beyond half filling, the peak at $Qa = \pm\pi$ becomes a dip. This effect, which we will refer to as *peak to dip transition*, has its origin in the occupation of the second band with few atoms, once the first band is fully occupied. In fact, it can be interpreted as a manifestation of the fermionization of HCBs. The peak to dip transition is a

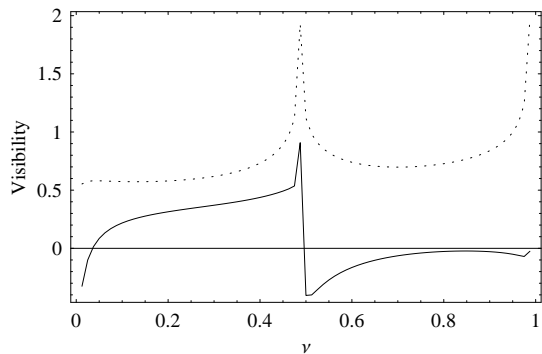


FIG. 3: Visibility (see text for definition) of the $Q = 0$ (dotted line) and $Qa = \pi$ (solid lines) peaks for a HCB system with $\lambda/J = 1$ and $L = 80$.

generic feature of strongly correlated bosons confined in a superlattice. It is seen for all values of λ and, as we discuss later, this signature also accompanies the onset to fractional Mott state for finite U , i.e. in the soft core boson case.

A further insight for this peak to dip transition can be gained by looking at the noise correlations as $\lambda \rightarrow \infty$. In this limit, the correlations can be calculated analytically for $\nu = 1$, $\nu = 1/2$ and also for the case of one extra atom beyond half filling ($N = L/2 + 1$). At unit filling the ground state in the HCB limit corresponds to a unit filled Fock state. In the half-filled case, to a good approximation, the ground state can be assumed to be a $1/2$ -filled Fock state $|\Psi_g\rangle = |1010\dots 10\rangle$. This is due to the reduced number fluctuations exhibited in this limit, as the tunneling between every two sites scales as $J^2/(4\lambda)$. At filling factor $N = L/2 + 1$ the ground state can be approximated by a $1/2$ -filled Fock state with an extra delocalized particle at the different unoccupied wells, $|\Psi_g\rangle = 1/\sqrt{L} \sum_{i=1}^N |i\rangle$, with $|i\rangle = |10\dots 11\dots 10\rangle$. Using these ansatzs, it can be shown that

$$\Delta(Q)_{N=L/2} = -\frac{1}{L} + \frac{1}{4}(3\delta_{Q0} + \delta_{Q\pi}), \quad (9)$$

$$\Delta(Q)_{N=L/2+1} = -\frac{1}{L} + \frac{1}{2}(3\delta_{Q0} - \delta_{Q\pi}), \quad (10)$$

$$\Delta(Q)_{N=L} = -\frac{2}{L} + 2\delta_{Q0}. \quad (11)$$

As shown by these equations, just beyond half-filling, the $Q = 0$ and $Qa = \pi$ fringes have opposite sign. The sign difference can be understood by calculating $\Delta(Q)$ for a single particle ($N = 1$) or a single hole ($N = L - 1$). In this simple case, noise correlations can be calculated explicitly for all values of λ :

$$\Delta(Q, 0)_{N=1=L-1} = \frac{1}{4} \left(\frac{\lambda^2}{\lambda^2 + 1} \right) (\delta_{Q0} - \delta_{Q\pi}). \quad (12)$$

The explicit formulas for $\Delta(Q, 0)_{N=L/2+1}$ and $\Delta(Q, 0)_{N=1}$ show on one hand the similarity between these two cases and on the other that the filled sub-band does have an effect on the extra particle. Actually as can be seen in Fig. 2 and 3, the

negative fringes survive even for more than one atom in the second band.

Eq.(11) also shows that the absence or the presence of an interference peak at $Qa = \pi$ can be used to distinguish the fractional and Mott insulating phases: the peak at $Qa = \pi$ disappears when the system is a unit filled insulator but continues to exist at $aQ = \pi$ when the system is a half-filled insulator. On the other hand, for both insulating phases the intensity of the central peak is $\nu(\nu + 1)$.

IV. SOFT CORE BOSONS

In this section we relax the hard-core constraint and explore the interplay between the finite interaction effects and the competing periodicity induced by the superlattice potential. The key questions that we address are: (1) how a finite value of U affects the various phases observed in the HCB limit, (2) how generic are the characteristic signals of the phase transitions observed in the HCB noise correlations as U becomes finite and (3) what novel characteristics of the interference pattern emerge as we explore the (J, U, λ, ν) parameter space.

Before we describe the details of HBTI, we will first use mean field theory to gain some insight about the phase diagram as $(U/J, \lambda/J, \nu)$ vary. Although previous studies based on numerical Monte carlo simulations have calculated the various phases in the soft core regime [14, 15, 16, 17, 18], here we obtain the phase diagram analytically by using second order perturbation theory. It is well known that the mean-field calculations provide a good characterization of the phase diagram and gives qualitative prediction of the different phase transitions even though the exact transition thresholds may not be quite correct. We would also like to point out that earlier mean field studies [14, 15, 16, 17] of the phase diagram were done in a different case, namely when the hopping parameter is site dependent.

A. Mean-Field Phase Diagram

To calculate the phase diagram we use the well know Gutzwiller approximation [27] that decouples the kinetic energy term of the Hamiltonian by introducing a superfluid order parameter. The details of the mean field calculations are discussed in Appendix A. Mean field theory predicts three insulating phases in addition to the superfluid phase. The insulating phases can be classified as: (1) a MI phase with $\nu = 1$ where all sites have unit occupancy, (2) a staggered MI phase with $\nu = 1$ characterized by every alternate site doubly occupied and (3) a fractional MI state with $\nu = 1/2$ where alternate sites are singly occupied. At other filling factors, the system is always a superfluid.

Fig. 4 summarizes the mean-field calculations. The top left panel shows the critical values of $\bar{U} \equiv U/J$ and $\bar{\lambda} \equiv \lambda/J$ for the onset to the three insulating phases. They correspond to the tips of the insulating lobes (multicritical points) that

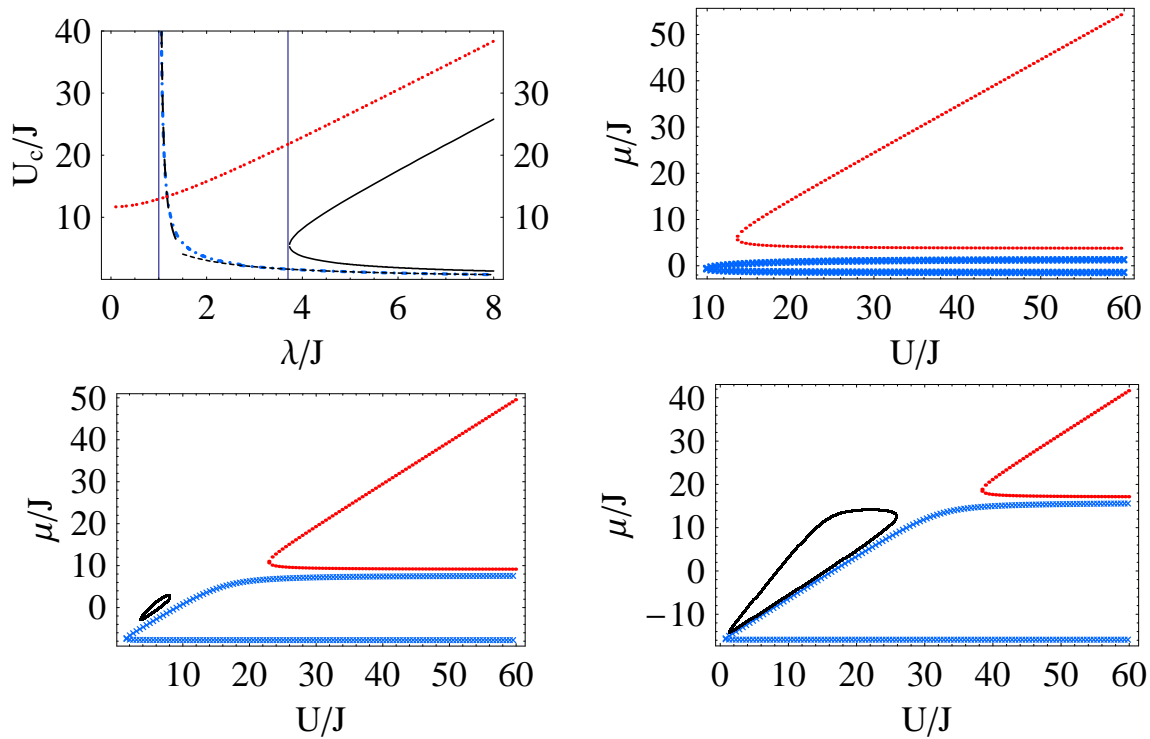


FIG. 4: (color online) Mean field phase diagram for the period two superlattice. The top left panel shows the critical curves, $U_c/J - \lambda_c/J$ for the onset to various transitions to insulating phases. The dash dotted blue line is for the transition to the band half-filled MI. The long dashed and short dashed asymptotes corresponds to $2.3/(\lambda/J - 1)$ and $6.1/(\lambda/J)$ respectively. The red dotted line corresponds to the transition to the unit filled MI and the black solid line to the staggered unit filled insulator. The grid lines are at $\lambda = J$ and 3.75 . The top right, bottom left and bottom right panels show the phase diagram as a function of the chemical potential for systems with $\lambda = 0.5J, 4J$ and $8J$.

are shown for selected values of $\bar{\lambda}$ in the various panels of the figure.

One of the interesting results of the mean-field theory is the prediction of a reentrance to the superfluid phase from the staggered MI phase. In contrast, to the critical curves describing the threshold to the fractional MI and integer MI phases, which vary monotonically in the $(\bar{U}, \bar{\lambda})$ space, the curve for the staggered MI at $\nu = 1$ bends (see left panel in Fig. 4) and becomes a double-valued function. As a consequence, for a fixed $\bar{\lambda} > \bar{\lambda}_c$, with the threshold value being approximately $\bar{\lambda}_c = 3.75$, as we increase the interaction \bar{U} , the system goes from superfluid to staggered MI, reenters the superfluid phase and ends in the unit filled MI phase. Note that this reentrance to the superfluid phase is absent for $\bar{\lambda} < \bar{\lambda}_c$, where one only sees a direct transition from superfluid to unit MI. This behavior is explicitly shown in the other panels of the figure where the chemical potential is plotted as a function of the interaction energy, for a few selected values of $\bar{\lambda}$. In the top right panel $\bar{\lambda} < \bar{\lambda}_c$ and so only the unit Mott and fractional Mott phases are present. For $\bar{\lambda} > \bar{\lambda}_c$, the staggered phase appears as an isolated island in the $\mu - U$ plane whose size grows with $\bar{\lambda}$.

The numerical Monte-Carlo calculations reported in Ref. [18] are in agreement with the intermediate superfluid phase found at mean-field level. However, according with their cal-

culations the superfluid region is only present for $\bar{U} < 12$. For $\bar{U} > 12$ the system is either a unit filled MI or a staggered MI. Our mean field calculations, on the other hand, predict that the intermediate superfluid phase exists for all values of \bar{U} . As we will discuss later, this result is in qualitative agreement with our numerical calculations performed by exact diagonalization of the BH Hamiltonian for finite size systems.

The staggered phase describes an interesting manifestation of the interplay between the onsite interaction energy, U , and the energy modulation introduced by the superlattice potential, λ . This phase is absent in the HCB limit and only exists for values of $\bar{\lambda} \equiv \lambda/J$ beyond a threshold value and for a finite window of $\bar{U} \equiv U/J$ values. The analytic calculations predict that the threshold value is $\bar{\lambda}_c = 3.75$, which is an overestimation of the corresponding value, $\bar{\lambda}_c \approx 1.75$, found with the Monte Carlo simulations [18].

For the half filled case, the mean-field critical curve has $1/\bar{\lambda}$ as an asymptote (see top left panel in Fig. 4). This scaling is consistent with Eq. (5) (for large $\bar{\lambda}$ the effective tunneling rate between consecutive odd sites goes like J^2/λ). Therefore, for large $\bar{\lambda}$, a fractional MI state can exist for rather small values of \bar{U} . On the other hand Fig. 4 shows that for moderate values of $\bar{\lambda}$ the transition to an insulating phase requires very large interactions. We would like to point out that the existence of a fractional Mott phase only for values of $\bar{\lambda} > 1$ seems to be

an artifact of the mean-field theory. In fact, in the HCB limit ($U \rightarrow \infty$) the system is a band insulator for any infinitesimal value of $\bar{\lambda}$.

B. Noise Correlations and Phase Diagram

To establish a correspondence between the various phase transitions and their signatures in noise-spectroscopy, we resort to exact diagonalization procedures. We first numerically diagonalize the BH system to obtain the ground state of the system. This is then used to obtain two and four point correlations and their Fourier transform. Here we will describe our results for 8 wells ($L = 8$).

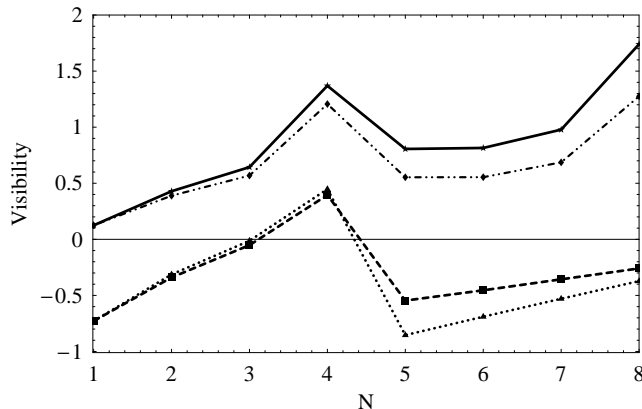


FIG. 5: For fixed $\lambda/J = 1$ and $U/J = 20$, we plot the visibility of the central (dotted-dashed line) and superlattice induced (dashed lines) peaks as the filling factor varies. The solid and dotted lines are the correspondent HCB curves

Fig. 5 describes the visibility [Eq. (8)] of the second order fringes for various filling factors. The important point to be noticed here is that the peak to dip transition, a key signature of the fractional Mott transition in the HCB limit, is preserved for finite U . The figure also shows the corresponding result for the HCB case. A comparison between the $L = 80$ (Fig. 3) and $L = 8$ results for HCB illustrates the finite size effect on the peak to dip transition. As expected, the finite size of the system broadens the transition and hence reduces the visibility of the interference peaks. Fig. 6 further demonstrates the behavior of the peak to dip effect as the interaction U is varied. In Fig. 6 we plot the normalized HBTI pattern as a function of \bar{U} for a system just above half filling. For large but finite $\bar{U} \gtrsim 10$, the superlattice induced peak in $\Delta(Qa = \pi)$ changes sign and becomes a dip. Our numerical analysis confirms that the peak to dip transition is a generic signature of the strongly interacting regime where bosons exhibit fermion-type characteristics.

We next show that the second order interference pattern not only complements the characteristics of the various phase transitions as observed in the first order Bragg spectroscopy, but it also provides new definitive signatures of various phases. For clarity, we will describe our results for $\nu = 1$ and

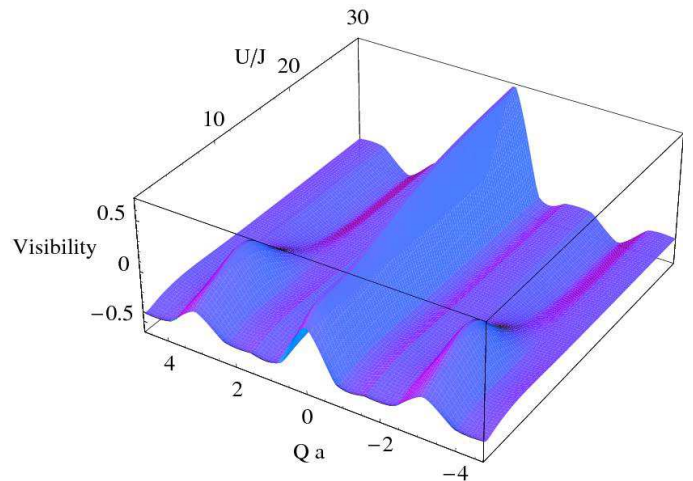


FIG. 6: Visibility plot (see text for definition) as a function of U/J for a system just beyond half filling ($L = 8$, $N = 5$) and for $\bar{\lambda} = 2$.

$\nu = 1/2$ separately.

(B.I) Unit-Filled Case

Fig. 7 shows the variation in the central as well as in the superlattice induced peak for both the first and the second order interference patterns as the on-site repulsive interaction is varied. An important aspect of the figure is the appearance of various local maxima in $\Delta(0)$. The single maximum observed for small $\bar{\lambda}$ splits as $\bar{\lambda}$ increases. A comparative study between $N = 6$ and 8 shows that the height at the various maxima increase with N , suggesting that it may be divergent in the thermodynamic limit. This observation along with the fact that the peak for small $\bar{\lambda}$ occurs at a value of \bar{U} very close to the well known MI transition, suggests that the maxima may be associated with the onset of the various superfluid to MI phase transitions.

By monitoring the locations of the maxima, we obtain the phase diagram in the $(\bar{U}, \bar{\lambda})$ plane. Our results are shown in Fig. 8. The rather remarkable qualitative agreement between this phase diagram and that obtained by mean-field and also by earlier Monte carlo studies, supports the validity of our conjecture regarding the relationship between a peak in $\Delta(0)$ and the onset of a phase transition, and suggests that noise correlations can be used as a practical tool to obtain phase diagrams of many body quantum systems. It should be noted (Fig. 7) that in contrast to $\Delta(0)$, the corresponding zero quasimomentum component does not provide any sharp signatures of the different critical points as U is varied.

As shown in the figure for $\bar{\lambda} = 3$, for moderate on-site interaction, the system is in the superfluid phase. As \bar{U} increases, correlations begin to build up and when U becomes comparable to J , for $\bar{\lambda} > 1.5$, the system enters the staggered Mott insulating phase with two atoms in the low energy wells and none in the high energy ones. The onset to this transition is signaled by a peak in $\Delta(0)$ (as seen in the figure) and by the development of a positive intensity peak at $Qa = \pi$. It

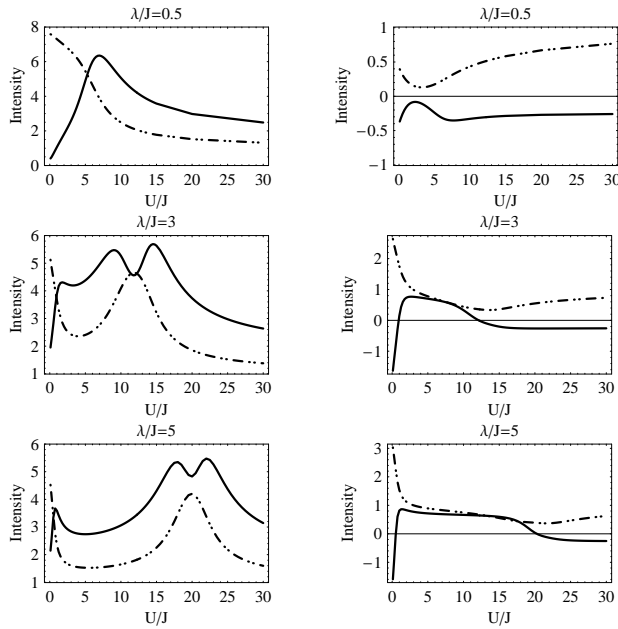


FIG. 7: The figure shows the noise correlations (solid line) and quasimomentum fridges (dashed line) for various $\bar{\lambda}$ values. The left and right panel respectively describe the intensities of the central peak ($Q = 0$) and the superlattice induced peak ($Qa = \pi$).

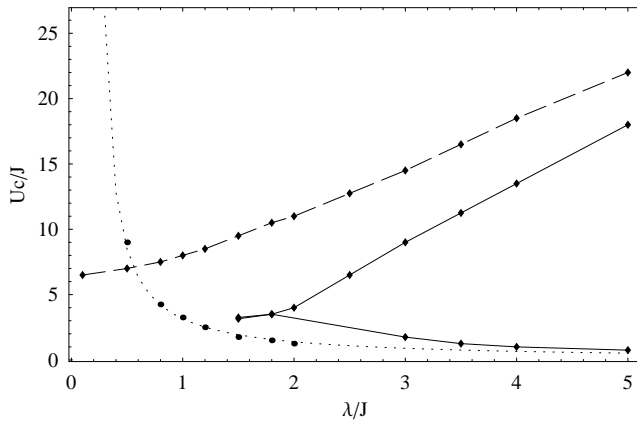


FIG. 8: Phase diagram for the period two superlattice calculated by reading the maxima of the central peak in the $\Delta(0)$ vs. \bar{U} plot for different $\bar{\lambda}$. The dotted, dashed and solid lines show the critical values in the \bar{U} vs $\bar{\lambda}$ plane for the transition to the half-filled MI, the unit filled MI and staggered filled insulators respectively.

should be noted that the critical value of $\bar{\lambda} = 1.5$ predicted by this method for the appearance of the staggered phase is very close to the value of 1.75 found by the numerical Monte-Carlo calculations [18].

The system continues to be in the staggered insulating phase as \bar{U} increases until the point when the competition between \bar{U} and the energy offset induced by the superlattice, $4\bar{\lambda}$, drives the system back to a superfluid phase. A simple

understanding of this reentrance can be obtained by realizing that when \bar{U} is of the order of $4\bar{\lambda}$ the state $|2020\dots\rangle$ is degenerated with the states $|20112011\dots\rangle$, $|10211021\dots\rangle$, $|21102110\dots\rangle$, and $|11201120\dots\rangle$ which have superfluid character as their average densities are $3/2$ and $1/2$ in the low and high energy wells respectively. The reentrance to the superfluid phase is signaled by the second peak in $\Delta(0)$. Furthermore, it is accompanied by the disappearance of superlattice induced peak at $Qa = \pi$. For values of $\bar{\lambda}$ close to 1.5 the staggered phase exist only for a very narrow range of \bar{U} values and the first and second order peak can not be resolved.

As \bar{U} increases beyond $4\bar{\lambda}$, it is energetically costly to have two atoms in the same well and hence the system enters the MI phase where sites are singly occupied. This transition is also signaled by the third peak in $\Delta(0)$. As $\bar{\lambda}$ is increased from 1.5 up to $\bar{\lambda} \approx 5$, the separation between the last two maxima (which determines the range of \bar{U} values where the intermediate superfluid phase exists) decreases. Beyond this value, as $\bar{\lambda}$ is increased further the position of the two peaks is shifted to larger values of \bar{U} . However, the relative separation between the peaks was found to remain constant. This finding is in disagreement with the results of Monte Carlo simulations which find points in $\bar{U} - \bar{\lambda}$ space where staggered and Mott phases coexist. One may argue that the absence of coexistence between the staggered and Mott phase in our analysis may be due to the finite size of our system. Nevertheless, the coexistence of such phases seems to imply the existence of a first order transition. This makes such a coexistence point somewhat subtle and needs further investigation. Besides this difference, the phase diagram calculated by monitoring the maxima in $\Delta(0)$ is in very good qualitative agreement with the Monte carlo as well as the mean field calculations. The quantitative differences are due to finite size effects.

We would like to point out that $\Delta(Q = \pi/a)$ also contains valuable information about the different phases. For example the existence of a staggered phase is indicated by the development of a positive interference peak at $Qa = \pi$. This peak is a second order effect and it is not present in the quasimomentum distribution. The quasimomentum distribution does not give definite signatures of the transition points but it gives information about the phase coherence of the various phases. As shown in Fig. 7, inside the superfluid phases the $n(0)$ vs \bar{U} develops a maximum which disappears in the insulating phases where the curve tends to become flat.

(B.II) Half filled Case

We next discuss the $\nu = 1/2$ case, where one sees a transition from superfluid to fractional Mott phase. The formation of this phase is also signaled by the development of a sharp peak in the intensity of the central noise correlation peak as \bar{U} is varied across the transition. This is shown in Fig. 9. In our finite size system, the peak was found to exist only for values of $\bar{\lambda} \gtrsim 0.205$. However, we expect this value to decrease as the size of the system increases. Fig. 8 shows the position of the peak as a function of $\bar{\lambda}$. For large $\bar{\lambda}$ the critical \bar{U} value decreases as $1/\bar{\lambda}$ in consistency with the mean field results.

The formation of the half filled band insulator is also

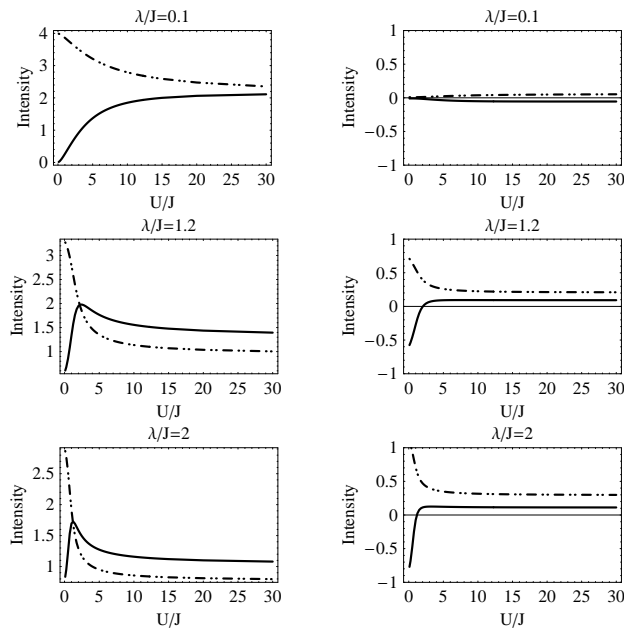


FIG. 9: The figure shows the noise correlations (solid line) and quasimomentum distribution (dashed line) for $\nu = 1/2$ and various $\bar{\lambda}$ values. The left and right panel respectively describe the intensities of the central peak $Q = 0$ and the superlattice induced peak ($Qa = \pi$).

indicated by the superlattice induced peak at $\Delta(\pi/a)$. It should be noted that $\Delta(\pi/a)$ has negative intensity for the non-interacting system. Precisely at $U = 0$ $\Delta(\pi/a) = -N/4\lambda^2/(\lambda^2 + J^2)$. Its amplitude increases as \bar{U} is increased and becomes positive for the values of $\bar{\lambda}$ that allow the formation of a band-insulator. For $\bar{U} > \bar{U}_c^{\nu=1/2}$, with $\bar{U}_c^{\nu=1/2}$ the Mott band insulator critical point, the peak intensity almost reaches its hard-core value.

V. TRAPPED SYSTEM

In this section we study the experimentally relevant case of a superlattice in the presence of an additional parabolic potential. The two key results of this study are following: First, to find that in contrast to the homogeneous system where the MI phases only exist at specific critical fillings, the trapping potential stabilizes the MI phases and allows for their existence over a large range of filling factors. Second, to show that noise-spectroscopy provides a detailed information of the formation of the insulating domains and the shell structure that arises in presence of a parabolic confinement.

Understanding the effects of the trap on period-2 superlattice follows along the lines of the earlier studies of the trapped system in the absence of any additional lattice modulation. Therefore, we first briefly review the key aspects of the $\lambda = 0$ case which has been studied in great detail [28, 29, 30, 31]. The combined lattice plus harmonic confinement system pos-

esses two distinct classes of eigenstates: low energy states that extend symmetrically around the trap center and high energy states that are localized on the sides of the potential. The origin of these two distinct classes is related to the two energy scales in the system, namely the tunneling (J) and the trapping energy (Ω). Modes with excitation energy below $4J$, which correspond to the band width of the translationally invariant system, are extended and can be thought of as harmonic oscillator like modes with effective frequency $\omega^* = \sqrt{4J\Omega}$ and effective mass $m^* = \hbar/(2Ja^2)$. Modes with excitation energies above $4J$ are close to position eigenstates since for these states the kinetic energy required for an atom to hop from one site to the next becomes insufficient to overcome the potential energy cost. The high energy eigenstates are almost two-fold degenerate with energy spacing mostly determined by Ω . The localization of these modes can be understood by means of a semiclassical analysis [29]. Within WKB scheme, the localization of the higher energy modes can be linked to the appearance of new turning points related to umklapp processes. In contrast to the turning points of the classical harmonic oscillator that appear at zero quasimomentum, the Bragg turning points emerge when the quasimomentum reaches the end of the Brillouin zone and can therefore be associated with Bragg scattering induced by the lattice.

The period-2 superlattice splits a band into two subbands and hence the nature of modes can be now classified by the energy scales associated with these two bands and the band gap which is equal to 4λ .

In the top panel of Fig.10 we plot the various wave functions. Each eigenstate has been offset along the y axis by its energy in units of $\sqrt{J\Omega}$. In the lower panel we also show the energy spectrum. As shown in the figure, we now see two sets of extended and also two sets of localized states. Again, the localized states are related to umklapp processes and to emphasize this idea, the classical and the Bragg turning points of both bands are explicitly displayed. In Appendix B, we provide additional details of the trapped superlattice model.

Figs. 11 and 12 describe the density and number fluctuations that reflect the band structure of the trapped superlattice system discussed above. To simplify the description, we introduce three different quantities: N_1^{LE} , N_1 and N_2^{LE} which respectively denote the number of low energy extended states in the first band, the number of states below the first mode of the second band and the total number of modes below the first localized mode of the second band. In Fig. 10, these three number are explicitly indicated with grid lines.

For filling factors below N_1^{LE} atoms tend to spread over the central sites populating mostly the low energy wells. The extended character of the modes induce large number fluctuations. For filling factors between $N_1^{LE} < N \leq N_1$, the localized modes in the first band become occupied. Because these modes are localized at the edges of the cloud, as the number of atoms is increased the occupation of the central site remains constant and instead sites farther away from the trap center become populated. Thus the presence of single-particle localized modes in the Fermi sea leads to the formation of fractionally filled insulating domains at the trap center in the many-body system. Alternatively, as soon as localized

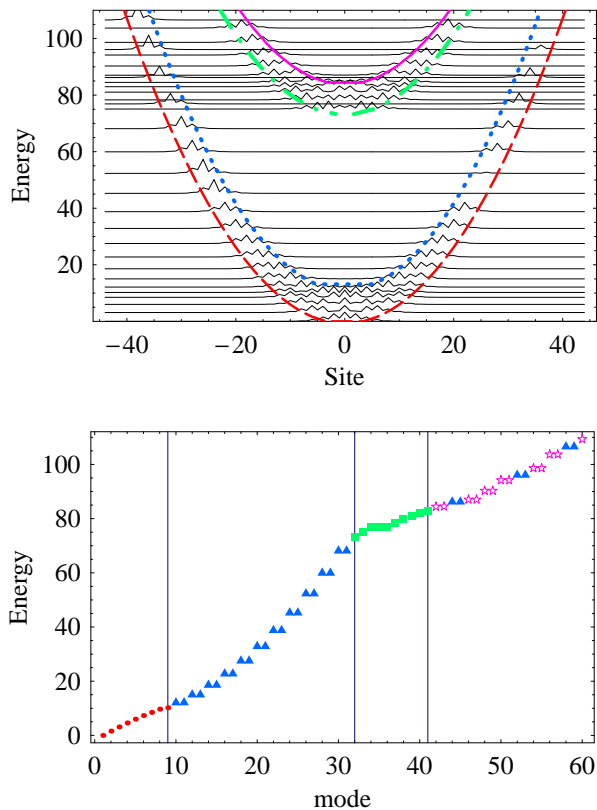


FIG. 10: (color online) The top panel shows the single-particle eigenstates of a system with $\lambda/J = 1.1$ and $\Omega/J = 0.005$. The height of each mode is proportional to its energy in units of $\sqrt{\Omega J}$. The parabola correspond to the classical and Bragg turning points that appear in the first and second band respectively (see text). In the lower panel we show the spectrum of the modes in units of $\sqrt{\Omega J}$. The dots, triangles, boxes and stars indicate the low energy modes in the first band, the high energy localized modes in the first band, the low energy modes in the second band and high energy localized modes in the second respectively. Note the degeneracy that appears between the localized high energy modes of the two bands. The grid lines are at $N_1^{LE} = 9$, $N_1 = 32$ and $N_2^{LE} = 42$.

modes are populated, number fluctuations become only relevant at the edges. The insulator character of the atoms at these central sites and the reduced number fluctuations can be seen in Fig.12.

For $N > N_1$ the trapping energy cost of placing an atom at the trap edge is higher than the energy needed to place the atom at the center. For $1 < N < N_2^{LE}$, atoms occupy the extended modes of the second band and tend to spread over the different empty sites at the trap center. When the number of atoms $N = N_2^{LE}$, the first localized mode of the band is populated and the site at the trap center acquires filling factor one. As N is further increased, the width of the unit-filled central core grows. For $N > N_2^{LE}$ the density profile alternates from unit filled MI, superfluid, fractional MI and superfluid as one moves from the center towards the edge of the cloud. This shell structure in the HCB limit resembles in many aspects

the shell structure observed in the $\lambda = 0$ case at moderate values of U . In the former case, the gap is induced by the external modulation and the shells consist of fractional and unit filled insulator domains surrounded by superfluid regions. In the later case, the gap is induced by the onsite interaction energy U and the shells consist of integer filled MI domains surrounded by superfluid regions.

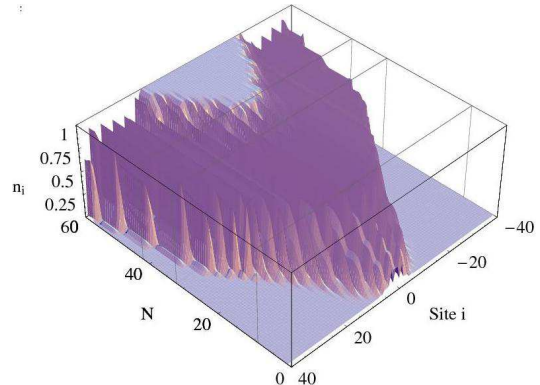


FIG. 11: (color online) Density distribution for a system with $\bar{\lambda} = 1.1$ and $\Omega/J = 0.005$ as a function of the total number of atoms. The grid lines are at $N_1^{LE} = 9$, $N_1 = 32$ and $N_2^{LE} = 42$.

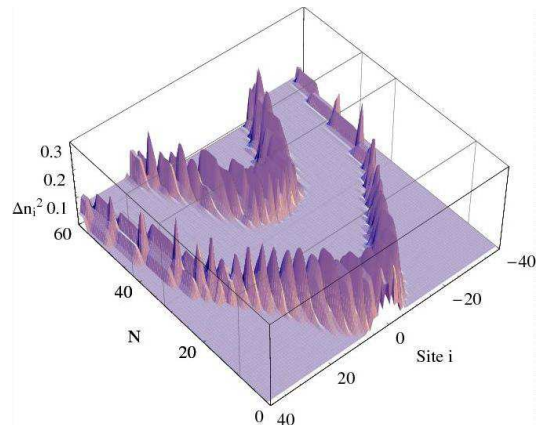


FIG. 12: (color online) Number fluctuations in the presence of trap for a system with $\bar{\lambda} = 1.1$ and $\Omega/J = 0.005$ as a function of the total number of atoms. The grid lines are at $N_1^{LE} = 9$, $N_1 = 32$ and $N_2^{LE} = 42$.

We now describe the first and second order interference patterns in the trapped system. The quasimomentum distribution is shown in Fig. 13. Consistent with the behavior observed in the density and number fluctuations, for filling factors $N < N_1^{LE}$ and $N_1 < N < N_2^{LE}$ the quasimomentum distribution is sharply peaked at $Q = 0$ and $Qa = \pi$, signaling the superfluid character of the system. The insulating phases that appear for filling factor $N_1^{LE} < N < N_1$ and $N > N_2^{LE}$ are signaled in the quasimomentum distribution by the drop of the peak intensities and the flattening of the quasimomentum distribution profile.

Fig. 14 shows the HBTI pattern for a different total number

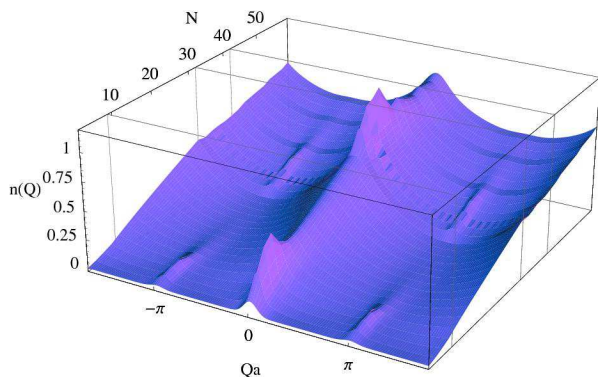


FIG. 13: (color online) Quasimomentum distribution for a system with $\lambda/J = 1.1$ and $\Omega/J = 0.005$ as a function of the filling factor. The grid lines are at $N_1^{LE} = 9$, $N_1 = 32$ and $N_2^{LE} = 42$.

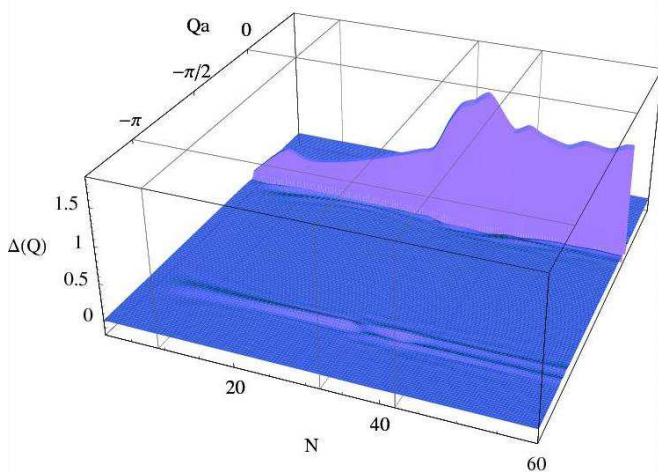


FIG. 14: (color online) Noise interference pattern as a function of the filling factor of a system with $\lambda/J = 1.1$ and $\Omega/J = 0.005$. The grid lines are at $N_1^{LE} = 9$, $N_1 = 32$ and $N_2^{LE} = 42$.

of atoms. For $N < N_1^{LE}$, only extended modes are occupied and the intensity of the central peak grows monotonically with N . Similarly the peak at $Qa = \pi$ increases from the negative value it takes for $N = 1$ and becomes a peak with a positive intensity. As the localized modes enter the Fermi sea ($N > N_1^{LE}$) the rate of growth of the central peak slows down and this change in the slope generates a maximum in the interference pattern. Note that in contrast to the strong reduction observed in the $\Omega = 0$ HCB case, in the presence of the trap only a decrease in the rate of growth is observed. The reason of this behavior is the fact that in the trapped case there is always a superfluid component at the edges of the atomic cloud. For $N_1^{LE} > N \geq N_1$ the interference peak at $qa = \pi$ is clearly visible, reflecting the staggered character of the phase.

At $N = N_1 + 1$, we see a rather sharp peak to dip transition at $Qa = \pi$. Similar to the homogeneous system, the transition signals the beginning of the population of an empty band. The dip becomes a peak when the number of atoms increases beyond a certain value. For $N_1 < N \leq N_2^{LE}$, one also observes an increase in the growth rate of the central peak with

N , consistent with the superfluid properties of the system at these fillings. Finally for $N > N_2^{LE}$, a unit filled insulating domain at appears at the trap center. This leads to a decrease in the amplitude of the central peak until it reaches a constant value. The peak at $Qa = \pi$ disappears as the unit filled core at the trap center grows. In the regime $N > N_2^{LE}$, Fig. 10 shows some additional small modulations of the central peak amplitude at certain fillings. The oscillations take place when a high energy mode of the first band, degenerated with another high energy mode of the second band, enters the Fermi sea.

In analogy with the homogeneous case, the transition to insulating state can best be illustrated in the normalized intensity of the noise correlations, namely the visibility. In Fig. 15, we plot the visibility of the central and the superlattice peaks. As mentioned above, the normalized pattern is perhaps the best experimental observable as the normalization procedure filters some of the technical noise introduced in the measurement procedure. The normalization procedure maps the central peak maxima that appear before the formation of the insulator domains to minima. Furthermore, when normalized, the amplitude of the superlattice induced peak becomes comparable in intensity to that of the central peak.

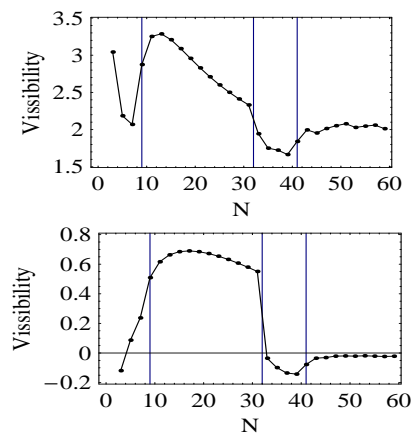


FIG. 15: Visibility of the second-order interference peaks at $Q = 0$ (top panel) and $Qa = \pi$ (bottom panel) as the total number of trapped atoms is varied. The grid lines are at $N_1^{LE} = 9$, $N_1 = 32$ and $N_2^{LE} = 42$.

VI. CONCLUSIONS

In this paper, we have studied shot noise correlations for interacting bosons in the presence of an additional lattice. Although we have focused on a period-2 superlattice, this simple case exhibits all the key aspects of the phase diagram of more general superlattice potentials.

One of the central results of this paper is that noise correlations may provide a practical tool to construct the phase diagram of many body quantum systems exhibiting transitions from superfluid to fractional and integer Mott phases which also include the staggered insulating phase. Our study sug-

gests that the intensity of the second order Bragg peaks provides a new order parameter to characterize these phase transitions. Although our calculations in the soft core regime were done for systems with a reduced number of atoms and wells and further studies for larger systems are needed to confirm our conjecture, we believe that this result is important in the theory of quantum phase transitions. Furthermore, our study of the trapped system demonstrates the possible realization of these phases in the laboratory.

Shot noise spectroscopy has already proven to be a useful experimental tool to identify Mott insulating states. We consider our analysis of the shot noise and its possible relevance in identifying various phase transitions in interacting bosons in superlattices is pertinent for atom optics experiments. Up to date all the experiments in super-lattice has been restricted to the Bose-Einstein-condensate regime. However, ongoing experimental efforts are trying to reach the strongly correlated regime in superlattices. The motivation of these efforts is not only to gain understanding of the many-body physics but also because atoms selectively loaded in super-lattices can have wider separation and stronger confinement, useful properties for the implementations of lattice based quantum computing proposals. We hope that our study will stimulate further experimental probing of one dimensional bosonic systems loaded in superlattices via HBTI.

VII. APPENDIX A

To study the phase diagram for the homogeneous system we use the well know decoupling approximation [27] and substitute:

$$\hat{a}_i^\dagger \hat{a}_j = \psi_i \hat{a}_j + \psi_j \hat{a}_i^\dagger - \psi_i \psi_j \quad (13)$$

into the BH Hamiltonian. Here $\psi_j = \langle \hat{a}_j \rangle \approx \sqrt{n_j}$ is the superfluid order parameter and n_j is the expectation value of the number of particles on site i . We will assume the order parameter to be real. This substitution leads to :

$$\begin{aligned} \hat{H}^{ef} = & -J \sum_j (\psi_{j+1} + \psi_{j-1}) (\hat{a}_j^\dagger + \hat{a}_j - \psi_j) \\ & + \sum_j (2\lambda \cos[\pi j] - \mu) \hat{n}_j + \frac{U}{2} \sum_j \hat{n}_j (\hat{n}_j - 1), \end{aligned} \quad (14)$$

where we have also introduced the chemical potential μ . Assuming periodic boundary conditions, one can reduced the problem to a two mode system due the fact that the Hamiltonian is exactly the same for all even and all odd sites. We define $\psi_2 = \psi_{2i}$, $\psi_1 = \psi_{2i+1}$, $\hat{a}_2 = \hat{a}_{2i}$ and $\hat{a}_1 = \hat{a}_{2i+1}$, so

$$\hat{H}^{ef} = \frac{N}{2} (\hat{H}_1^{ef} + \hat{H}_1^{ef}), \quad (15)$$

$$\begin{aligned} \hat{H}_1^{ef} = & -2J\psi_2 (\hat{a}_1^\dagger + \hat{a}_1 - \psi_1) \\ & - (2\lambda + \mu) \hat{n}_1 + \frac{U}{2} \hat{n}_1 (\hat{n}_1 - 1), \end{aligned} \quad (16)$$

$$\begin{aligned} \hat{H}_2^{ef} = & -2J\psi_1 (\hat{a}_2^\dagger + \hat{a}_2 - \psi_2) \\ & + (2\lambda - \mu) \hat{n}_2 + \frac{U}{2} \hat{n}_2 (\hat{n}_2 - 1). \end{aligned} \quad (17)$$

The above Hamiltonian can be diagonalized using a Fock state basis truncated below a certain occupation value. However, second order perturbation theory using ψ as an expansion parameter can provide a good analytic approximation of the phase diagram. At zero order in ψ the Hamiltonian is diagonal in the Fock basis. The integer occupation numbers n_1, n_2 that minimized the energy are given by the conditions

$$n_1 - 1 < \frac{\mu + 2\lambda}{U} < n_1, \quad (18)$$

$$n_2 - 1 < \frac{\mu - 2\lambda}{U} < n_2. \quad (19)$$

We consider three different cases:

- $-2\lambda < \mu < \min(U - 2\lambda, 2\lambda)$

In this case the ground state of the system is the Fock State $|010101 \dots\rangle$ and the unperturbed energy is $E_g^{(0)} = -2\lambda - \mu$. The first order correction to the energy vanishes and to second order one gets:

$$E_g^{(2)} = 4J \left(\frac{J\psi_1^2}{\mu - 2\lambda} - \frac{J\psi_2^2}{\mu + 2\lambda} + \frac{2J\psi_2^2}{\mu + 2\lambda - U} + \psi_1 \psi_2 \right) \quad (20)$$

Minimizing the energy respect to $\psi_{1,2}$ yields the following equation:

$$\begin{pmatrix} 1 & \frac{2J}{\mu - 2\lambda} \\ \frac{2J(\mu + 2\lambda + U)}{(\mu + 2\lambda - U)(\mu + 2\lambda)} & 1 \end{pmatrix} \begin{pmatrix} \psi_2 \\ \psi_1 \end{pmatrix} = \begin{pmatrix} 0 \\ 0 \end{pmatrix}. \quad (21)$$

Eq. (21) has nontrivial solution only when the determinant of the matrix vanishes. Therefore the surface where the determinant vanishes determines the insulating phase:

$$4J^2(\bar{\mu} + 2\bar{\lambda} + \bar{U}) = (\bar{\mu} + 2\bar{\lambda} - \bar{U})(\bar{\mu}^2 - 4\bar{\lambda}^2), \quad (22)$$

where the bar denotes the dimensionless variables $\bar{U} = U/J$, $\bar{\lambda} = \lambda/J$ and $\bar{\mu} = \mu/J$. In Fig. 4 we show, with a crossed blue line, the solutions of Eq. (22) in the $\bar{\mu}$ vs. \bar{U} plane, for $\bar{\lambda} = 0.5, 4$ and 8 (top right, bottom left panel and bottom right panels respectively). The region inside the blue loops corresponds to the $1/2$ filled insulator. In the top left panel we also show with a blue dash-dotted line the critical value of $\bar{U}_c^{\nu=1/2}$ as a function of $\bar{\lambda}$. $\bar{U}_c^{\nu=1/2}$ corresponds to the smallest \bar{U} in the lobe, below which the system is always a superfluid. Exactly at $\bar{U}_c^{\nu=1/2}$ the upper and lower branches of the chemical

potential merge and the energy gap closes up. It is important to point out that in general mean field calculations do not accurately predict critical values but, in general, they capture very well the physics of the phase transition.

- $2\lambda < \mu < U - 2\lambda$

In this case the ground state of the system is the unit filled state with exactly one atom per site. The zero order ground state energy is $E_g^{(0)} = -2\mu$. For this case we set $\psi_1 = \psi_2 = \psi$. To second order the ground state energy is given by:

$$E_g^{(2)} = \left(\frac{8J^2\psi^2}{\mu - 2\lambda - U} + \frac{8J^2\psi^2}{\mu + 2\lambda - U} \right) - \left(\frac{4J^2\psi^2}{\mu + 2\lambda} + \frac{4J^2\psi^2}{\mu - 2\lambda} \right) + 4J\psi^2. \quad (23)$$

Minimizing with respect to ψ one gets an algebraic equation that determines the boundary between the superfluid and insulating phases. The solution is displayed in Fig.4 for $\bar{\lambda} = 0.5, 4$ and 8 . The critical value of $\bar{U}_c^{\nu=1}$ is also shown in the top left panel with a dotted red line. Note the critical value increases with $\bar{\lambda}$. This increase is in agreement with the idea that for weak interactions disorder helps to delocalize the atoms.

- $U - 2\lambda < \mu < 2 \min(U - \lambda, \lambda)$

In this case the on-site repulsion is not large enough to avoid double occupancies and the ground state of the system is the state with two atoms in the low energy sites and zero in the others. This situation can not be described in the hard core regime and it is only present at moderate values of U . To zero order in J , the ground state energy is $E_g^{(0)} = -2\mu - 4\lambda + U$. To second order it is given by

$$E_g^{(2)} = \frac{4J^2\psi_1^2}{\mu - 2\lambda - U} - \frac{4J^2\psi_1^2}{\mu + 2\lambda} + \frac{4J^2\psi_2^2}{2\lambda - \mu} + \frac{8J^2\psi_2^2}{\mu + 2\lambda - U} + 4J\psi_1\psi_2 \quad (24)$$

By first minimizing with respect to $\psi_{1,2}$, and finding the solutions for which the determinant vanishes one obtains the boundary for this phase. The solution is displayed in Fig.4 for $\bar{\lambda} = 0.5, 4$ and 8 with a black line. At mean field level the minimum value of $\bar{\lambda}$ required for the existence of this insulating phase is $\bar{\lambda} = 3.75$. For values of $\bar{\lambda} > 3.75$ the unit filled system is a superfluid for $\bar{U} < \bar{U}_{c1}^{\nu=1}$, a staggered insulator for $\bar{U}_{c1}^{\nu=1} < \bar{U} < \bar{U}_{c2}^{\nu=1}$ and a unit filled Mott insulator

for $\bar{U} > \bar{U}_{c2}^{\nu=1}$. In the top right panel, the lower and upper branches of the solid black curve correspond to $\bar{U}_{c1}^{\nu=1}$ and $\bar{U}_{c2}^{\nu=1}$ respectively.

VIII. APPENDIX B

The super-lattice potential splits the main band into two different sub-bands. In this "multi"-band picture, it is simple to understand the modification introduced by the trap. For excitation energies below the band width of the first sub-band: $E^{(n)} - E^{(0)} < E_{with}^{(1)} \equiv 2\sqrt{J^2 + \lambda^2} - 2\lambda$, the modes are delocalized states that spread every other site symmetrically around the potential minimum. In the semiclassical picture these modes only see the classical turning point at $x_{cla}^{(1)} = \pm a\sqrt{(E^{(n)} + 2\sqrt{\lambda^2 + J^2})/\Omega}$. For higher energies, $E^{(n)} - E^{(0)} \geq E_{with}^{(1)}$, the eigenstates become localized on both sites of the potential. These modes see besides the classical turning point, the Bragg turning point of the first band $x_B^{(1)} = \pm a\sqrt{(E^{(n)} + 2\lambda)/\Omega}$.

At excitation energies higher than 4λ (the energy gap between the two subbands), the potential energy cost of localizing a state at the edge is larger than the energy required to populate the high energy wells at the trap center. As a consequence, states with quantum number $n > \sqrt{4\lambda/\Omega}$ appear centered again around the trap minima. These second group of extended states see the classical turning point at $x_{cla}^{(2)} = \pm a\sqrt{(E^{(n)} - 4\lambda + 2\sqrt{\lambda^2 - J^2})/\Omega}$. Finally, for excitation energies larger than the band width of the second band $E^{(n)} - E^{(0)} \geq E_{with}^{(2)} = E_{with}^{(1)}$, the modes feel the Bragg turning point of the band $x_B^{(2)} = \pm a\sqrt{(E^{(n)} - 2\lambda)/\Omega}$ and become again localized at the edge. Sometimes a high energy mode in the second band becomes degenerated with some of the very high energy modes of the first band. This effect can be seen in Fig. 10.

Acknowledgments We would like to thank J.V. Porto, I.B. Spielman and S. Sachdev for their suggestions, comments and useful input. This work is supported in part by the Advanced Research and Development Activity (ARDA) contract and the U.S. National Science Foundation through a grant PHY-0100767. A.M.R. acknowledges support by a grant from the Institute of Theoretical, Atomic, Molecular and Optical Physics at Harvard University and Smithsonian Astrophysical observatory.

[1] Laburthe Tolra B *et al* 2004 *Phys. Rev. Lett.* **92** 190401 .
 [2] Kinoshita T, Wenger T and Weiss D S 2004 *Science* **305** 1125.
 [3] Paredes B *et al* 2004 *Nature* **429** 277.
 [4] Moritz H, Stöferle T, Köhl M and Esslinger T 2003 *Phys. Rev. Lett.* **91** 250402.
 [5] Fertig C D *et al* 2005 *Phys. Rev. Lett.* **94** 120403.

[6] Girardeau M 1960 *J. Math. Phys.* **1** 516 .
 [7] M. Fisher *et al*, *Phys. Rev. B* **40**, 546, (1989).
 [8] Markus Greiner, Olaf Mandel, Tilman Esslinger, Theodor W. Hansch and Immanuel Bloch, *Nature*, **415**, 39, 2002.
 [9] E. Altman *et al*, *New J. Phys* **5**, 113.1 (2003).
 [10] R. Hanbury Brown, R. Q. Twiss, *Nature* **177**, 27 (1956).

- [11] K. Drese and M. Holthaus, *Phys Rev Letter*, **78**, 2932, (1997).
- [12] S. Peil *et al* *Phys. Rev. A* **67**, 051603(R) (2003).
- [13] R. Roth and K. Burnett, *Phys Rev A*, **68**, 023604 (2003).
- [14] P. Buonsante and A. Vezzani, *Phys. Rev. A* **70**, 033608 (2004).
- [15] P. Buonsante *et al.*, *Phys. Rev. A* **70**, 061603 2004.
- [16] P. Buonsante, V. Penna, and A. Vezzani *Phys. Rev. A* **72**, 031602 2005.
- [17] P. Buonsante and A. Vezzani, *Phys. Rev. A* **72**, 013614 (2005).
- [18] V.G. Rousseau, *et al.*, *cond-mat/0601681*.
- [19] E. Altman *et al*, *Phys. Rev. A* **70**, 013603 (2004).
- [20] S. Foelling *et al*, *Nature* **434**,481 (2005).
- [21] Greiner M *et al* 2005 *Phys. Rev. Lett.* **94** 110401.
- [22] Jaksch D *et al* 1998 *Phys. Rev. Lett.***81** 3108.
- [23] A. M. Rey, I.I. Satija, and C. W. Clark *cond-mat/0511700* (J. Phys. B in press).
- [24] Holstein T and Primakoff H 1940, *Phys Rev.* **58** 1098.
- [25] Sachdev S 1999 *Quantum Phase Transitions* (Cambridge University Press).
- [26] Lieb E , Schultz T and Mattis D 1961 *Ann. Phys.* **16** 407.
- [27] K. Sheshadri, H. Krishnamurthy, R. Pandit and T. Ramakrishnan, *Europhys. Lett.* **22**, 257 (1993).
- [28] M. Rigol and A. Muramatsu, *Phys. Rev. A* **70**, 043627 (2004).
- [29] C. Hooley and J. Quintanilla, *Phys. Rev. Lett.* **93**, 080404 (2004).
- [30] H. Ott, E. de Mirandes, F. Ferlaino, G. Roati, V. Türck, G. Modugno, and M. Inguscio, *Phys. Rev. Lett.* **93**, 120407 (2004).
- [31] A. M. Rey, G. Pupillo, C.J. Williams and C. Clark, *Phys. Rev. A* **72**, 033616 (2005)